Materials and Structures (2024) 57:101
https://doi.org/10.1617/s11527-024-02387-x

ORIGINAL ARTICLE

Impact of triisopropanolamine on surface composition, crystallographic variation, and thermal behavior of C_3A polymorphs

Hyunuk Kang · Jihoon Lee · Jingwei Yang · Juhyuk Moon

Received: 2 January 2024 / Accepted: 5 May 2024 / Published online: 14 May 2024

Abstract In this study, the impact of triisopropanolamine (TIPA) on both the crystallographic and surface properties of cubic and orthorhombic tricalcium aluminate (C_3A) were investigated together with their hydration behavior and strength development. When TIPA was added during the grinding process, the pre-hydration and carbonation of C_3A were effectively prevented, and crystal structural changes of C_3A were confirmed. It leads to altering the hydration mechanism of C_3A phases: in the case of cubic C_3A, it promotes the formation of Al-hydrogarnet phases instead of OH-AFm phases even on the first day of curing. Similar hydration behavior was observed with orthorhombic C_3A, but the phase transition of OH-AFm phases to Al-hydrogarnet occurs during a specific time period in 1–3 days. The latter was revealed as a very interesting endothermic reaction which can be the only heat absorptive behavior in complex cement hydration as reported so far.

Keywords X-ray diffraction method · Triisopropanolamine · Tricalcium aluminate · Hydration mechanism

H. Kang · J. Lee · J. Yang · J. Moon (✉)
Department of Civil and Environmental Engineering, Seoul National University, Seoul 08826, Republic of Korea
e-mail: juhyukmoon@snu.ac.kr

J. Moon
Institute of Construction and Environmental Engineering, Seoul 08826, Republic of Korea

1 Introduction

Tricalcium aluminate (C_3A) is one of the primary clinker phases in ordinary Portland cement (OPC), and typically presents in amounts of 2–12 wt%. The crystal structure of cubic C_3A (c-C_3A or $Ca_3Al_2O_6$) can accommodate the Na^+ element, resulting in an orthorhombic C_3A (o-C_3A or $Na_xCa_{3-x}Al_2O_6$) polymorph [1–3]. This modification of c-C_3A's mineralogy can be also induced from a mechanism in which Ca^{2+} is partially replaced by Na^+. The clinker produced during the calcining process usually contains c-C_3A, but the phase can change to o-C_3A depending not only on the raw material used but also on the storage environment of OPC [2, 3]. With these intrinsic properties of C_3A, the hydration properties of C_3A also differ considerably depending on the type of polymorph [4–6].

The reactivity of both polymorphs of C_3A is significant within clinker, and it has been reported to have an impact on the initial hydration reaction of OPC [3, 7]. When water and C_3A come into contact, a substantial amount of hydration heat is generated, and significant quantities of hydration products (such as gibbsite (AH_3), Al-hydrogarnet (C_3AH_6), and OH-AFm (C_4AH_x) phases) are produced [6, 8]. Due to its high reactivity, it has been reported that C_3A can actively react with water under ambient conditions, which is known as the pre-hydration of OPC. Pre-hydration can affect the initial hydration properties of OPC, including its setting behavior

[9–11]. Therefore, inhibiting the effects of C_3A pre-hydration is quite important factor, as it can potentially alter the mechanical and hydration behaviors of OPC.

A grinding agent (GA) is typically added to OPC before the grinding stage to improve its grinding performance [12–15]. Moreover, the application of GA significantly changes the hydration behavior of clinker phases [16–19]. Alkanolamine-based GAs, such as triethanolamine (TEA), diethanol isopropanolamine (DEIPA), and Triisopropanolamine (TIPA), are widely used in the cement production. When TEA is used, the aluminate reactions (C_3A and ferrite [C_4AF]) are improved, suggesting that even a small amount of TEA can cause remarkable variations in the hydration mechanism of aluminate phases [16]. Similarly, DEIPA accelerates the aluminate reactions in the early stage, and it has been concluded that the complex hydration mechanism can affect the mechanical properties of concrete [19]. TIPA enhances the aluminate reactions, and it has been reported that the C_3A reaction is significantly improved with TIPA [20]. Based on this research, it is worth studying the variation of hydration reaction of C_3A according to different alkanolamine-based GAs in the base of different polymorphs of C_3A.

As mentioned above, it has been found that alkanolamine-based GAs can change the hydration characteristics of the C_3A phase [19]. However, the effects of alkanolamine-based GAs on the surface of C_3A and their impact on the hydration behavior of C_3A phases have not fully understood. Therefore, the aim of this study is to investigate the effects of two dosages (0.1% and 0.3%) of TIPA on the crystallographic variations and surface properties of C_3A, as well as the modification of the hydration and mechanical properties of C_3A caused by these effects. The investigation was carried out on the two different crystal structures of cubic and orthorhombic using X-ray diffraction (XRD) and X-ray photoelectron spectroscopy (XPS) to analyze the crystallographic variations and surface properties of C_3A induced by TIPA, respectively. In addition, inductively coupled plasma optical emission spectroscopy (ICP OES), isothermal calorimetry, thermogravimetric analysis (TGA), and quantitative XRD (QXRD) were used to investigate the hydration properties along with compressive strength measurement.

Table 1 QXRD results of unhydrated c-C_3A and o-C_3A

Phase	c-C_3A	o-C_3A
c-C_3A	100	–
o-C_3A	–	93.3
Calcium oxide	–	5.4
Calcium carbonate	–	1.3

Table 2 Mix design for C_3A powder (before grinding program)

Sample label	c-C_3A	o-C_3A	TIPA
c-C_3A_0%	100	–	–
c-C_3A_0.1%	100	–	0.1
c-C_3A_0.3%	100	–	0.3
o-C_3A_0%	–	100	–
o-C_3A_0.1%	–	100	0.1
o-C_3A_0.3%	–	100	0.3

2 Materials and experimental methods

2.1 Sample preparation

In this study, samples of c-C_3A and o-C_3A (Construction Technology Laboratories, Inc., Skokie, IL) were used. Pure TIPA was obtained from a Korean concrete admixture company (Silkroad, Seoul, Korea). The C_3A nodules were obtained by calcining at 1,300° for 2 h, and coarse C_3A powders were obtained by hand grinding for 5 min, followed by sieving under 500 μm. The QXRD results of c-C_3A and o-C_3A are provided in Table 1. The c-C_3A and o-C_3A series were distinguished by adding TIPA contents (0%, 0.1%, and 0.3%) before the grinding program (Table 2). The water-to-C_3A ratio for the paste was set to 1.0, with the water content adequately applied to the C_3A content.

2.2 Experimental method

In this study, lab-scale micro ball mill equipment (McCrone Micronizing Mill; McCrone Scientific Ltd., London, UK) was used to grind the C_3A

powder. The grinding conditions of C_3A (10 g) powder and the amount of TIPA (0%, 0.1%, and 0.3%) were determined based on several preliminary experiments. The grinding time and rotation speed were set to 14 min and 1,166 rpm, respectively. The particle size distribution was measured using a microparticle size analyzer (Malvern Instruments Ltd., Malvern, UK) with isopropyl alcohol, which does not react with C_3A, as the dispersion medium [21]. The effect of TIPA on the grinding degree of C_3A was evaluated based on these results.

In this study, an AXIS Supra + spectrometer for chemical analysis (Kratos Analytical Limited, Manchester, UK) was used to measure the XPS spectra. The measuring range was set from 0 to 1,200 eV, with data collected at one point per eV [22]. The sample pre-processing method was as follows: first, the powders were dehydrated for 24 h in a vacuum environment at 20 °C Then, the dried powders were molded into a 7 mm diameter pressed pellet and stored in a vacuum environment before the experiment started. XPSPEAK 4.1 software was used to analyze the XPS spectra, with a Shirley type background adopted due to the complexity of XPS spectra. The Gaussian–Lorentzian ratio function (3:2) was used to fit the peak position, full width at half maximum (FWHM), and area factors [23].

Five identical $10 \times 10 \times 10$ mm^3 paste specimens, where the water-to-C_3A ratio was 1:1, were chosen to determine the compressive strength of the specimens cured for 1 day and 3 days. Based on several preliminary tests with identical sizes of OPC specimens, a loading rate of 0.05 mm/min was carefully assigned.

ICP OES analysis was conducted using an Agilent 5100 SVDV ICP OES device (Agilent Technologies, Santa Clara, CA, USA). The water to C_3A ratio was set to 10:1 by weight. After 30 min of stirring, the solutions were filtered through a 200 nm filter. Prior to the experiment, the plasmid argon gas was subjected to an induction magnetic field, and the preprocessed liquid was sprayed onto the particles and injected [24].

To investigate the exothermic reaction between C_3A, TIPA, and water, a micro-calorimeter (TAM Air 8-channel, TA Instruments, New Castle, DE, USA) was used. The water-to-C_3A ratio was also set to 1:1 by weight. The device was calibrated before the experiment by holding it at a constant 20 °C for at least 24 h. After mixing 6 g of water and 6 g of C_3A powder for 1 min, the 5 g of resulting slurry was injected into the ampoule. The ampoule was then placed into the device. The heat flow and cumulative heat data were normalized to the amount of C_3A powder and water contained in the ampoule.

A D2 Phaser X-ray diffractometer (Bruker Co. Ltd., Land Baden-Württemberg, Germany) was used to measure the XRD patterns, with Cu Kα radiation ($\lambda = 1.5418$ Å) as the source. The tube current and generator voltage were set at 10 mA and 30 kV, respectively [25, 26]. For the samples that were hydrated for 1 day and 3 days, the hydration stop method was used. The detailed process is as follows: The paste samples that had cured for the specified periods (i.e., 1 day and 3 days) were ground for 10 min to attain fine powders. Isopropyl alcohol and diethyl ether were then used as exchange solutions to remove free water that was still present in the powders [27, 28].

The XRD patterns obtained were analyzed using TOPAS software version 7.0 (Bruker Co. Ltd., Land Baden-Württemberg, Germany). The background of the XRD patterns was corrected using the Chebyshev polynomial and 1/X terms equipped in TOPAS software. The scale, unit cell, and FWHM factors were the profiled fitting parameters [29, 30]. The internal standard method was used to analyze the hydration properties of C_3A. Al_2O_3 (NIST SRM 676a) was selected as the internal standard material because it does not overlap with the other crystals. C_3A powder and an internal standard material were mixed in a 1:9 ratio by weight, and the mixture was mixed for 30 min [28, 31, 32]. The Rietveld refinement method was then used to perform all of the quantitative evaluations for all crystalline phases. The quantified mineral phases were corrected using the amount of internal standard material added, which is shown in Eq. (1). The amount of amorphous phase was calculated using the actually added amount of internal standard material. Finally, the quantitative analysis results of all phases were calibrated using the value of chemically bound water (CBW), which will be mentioned later (Eq. (2)) [27].

$$\mathrm{Corr}\left(w_\alpha\right) = w_\alpha \frac{\mathrm{STD}_{\mathrm{known}}}{\mathrm{STD}_{\mathrm{measured}}} \tag{1}$$

$$w_{\text{amorphous}} = 1 - \sum_{j=1}^{n} \text{Corr}(w_j) \quad (2)$$

where $\text{Corr}(w_\alpha)$, w_α, $\text{STD}_{\text{known}}$, and $\text{STD}_{\text{measured}}$ indicate the corrected weight percentage of α, weight percentage of α, analyzed weight percentage of internal standard material, and analyzed weight percentage of internal standard material, respectively.

To obtain TGA data, a differential scanning calorimeter (DSC)-TG system (SDT Q600, TA Instruments Ltd., Newcastle, DE, USA) was used. The temperature range was from 30 °C to 1,000 °C, and the heating rate was 10 ℃ per minute [27]. In addition, the hardened paste samples underwent the hydration stop procedure at 1 day and 3 days, and 25–30 mg of powder was measured to analyze the hydration properties of each sample.

3 Results

3.1 Particle size distribution

Variations in the particle size distribution of the c-C_3A and o-C_3A series are presented in Fig. 1a, b. It is difficult to identify a clear trend with the c-C_3A series. However, a noticeable particle size reduction was confirmed with the o-C_3A series. When 0.1% of TIPA was added, a new first mode was detected, and the second mode was shifted to the left position. In addition, a weakened effect was exhibited with 0.3% TIPA compared to the sample with 0.1% TIPA. The results obtained are consistent with those reported in a previous study where a large amount of GA was added [33].

3.2 XPS results

Figure 2a, b shows the XPS results obtained from both C_3A polymorphs after the grinding process. Noticeable variations were observed according to the amount of TIPA added. In particular, variations in peak properties were observed in the scan ranges of ~ 72.5 eV and 290.0 eV, which correspond to the states of Al and C atoms, respectively.

Similar to previous studies, the Al 2p spectra of c-C_3A_0% and o-C_3A_0% showed two contributions, with the spectra located at 72.93 and 74.31 eV for c-C_3A_0% and at 73.34 and 73.94 eV for o-C_3A_0% [9, 34]. This difference indicates that the Al binding energies are closely related to the coordination number [35]. In the case of o-C_3A_0%, the replacement of Ca^{2+} by Na^{+} occurred, resulting in a difference in the binding energies of Al 2p. Meanwhile, an interesting trend was observed with the TIPA-added samples: the position of the Al 2p spectra shifted to a lower energy when the amount of TIPA added was increased. The binding energies of Ca 2p (346.48 to 346.93 eV) were almost identical and in good agreement with previous studies [9, 34]. With the Ca 2p spectra, it is difficult to observe a noticeable trend because the spectra are less susceptible to compositional variations (e.g., calcium aluminate hydrate and calcium silicate hydrate) [34, 36]. Detailed explanations will be provided later.

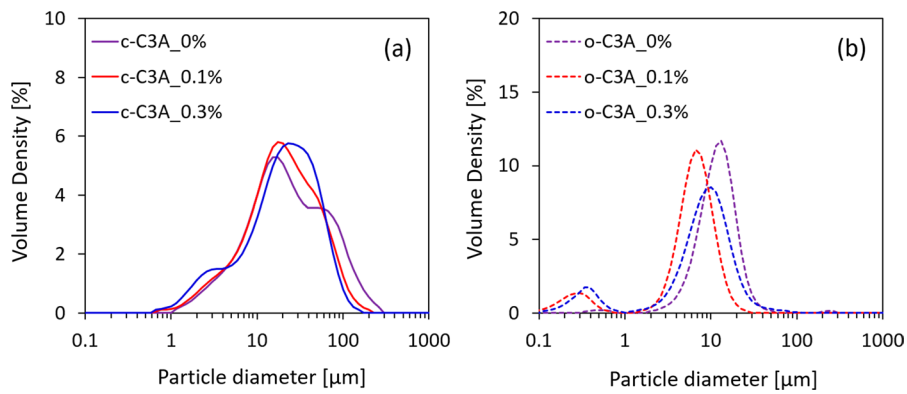

Fig. 1 Particle size distributions of **a** c-C_3A and **b** o-C_3A series

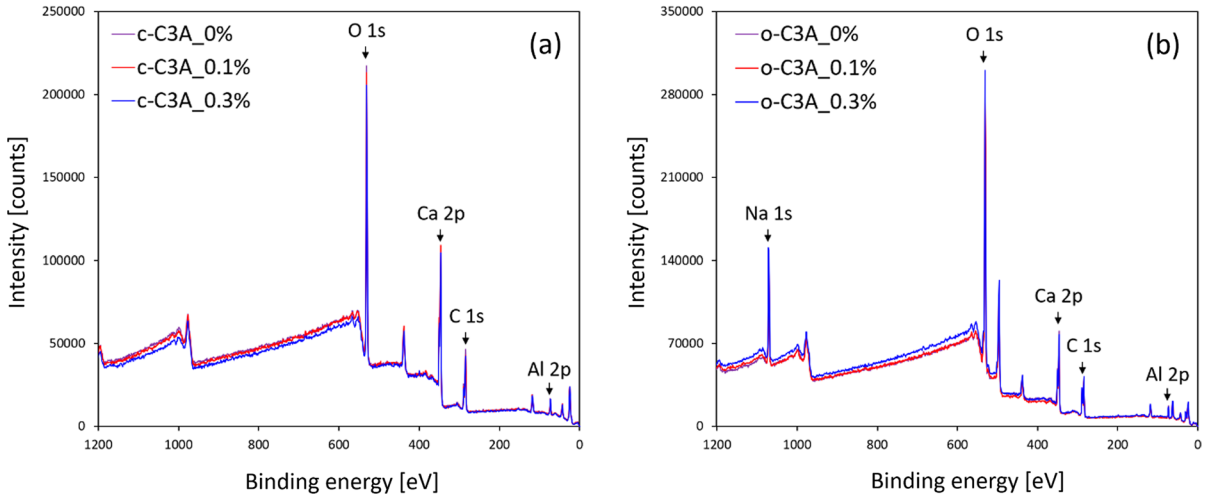

Fig. 2 XPS results of **a** c-C_3A and **b** o-C_3A series

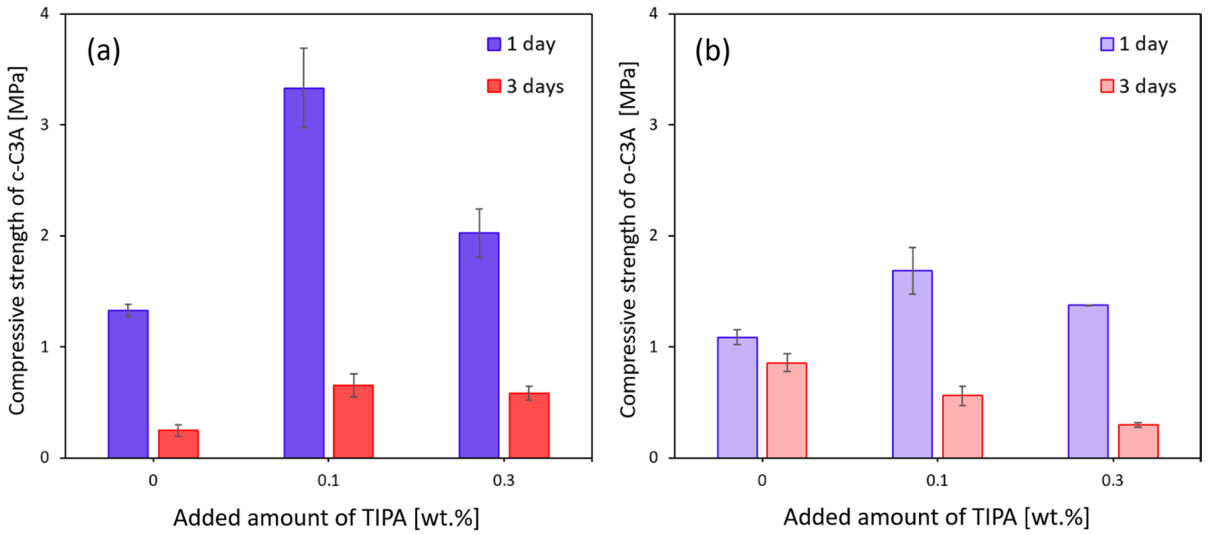

Fig. 3 Compressive strength results of **a** c-C_3A and **b** o-C_3A series

3.3 Compressive strength results

The compressive strength results of all C_3A pastes are presented in Fig. 3a, b. Overall, the compressive strengths of the c-C_3A series are higher than those of the o-C_3A series. When TIPA was added, the compressive strength of the samples cured for 1 day increased. In particular, a significant effect was observed in the samples with 0.1% TIPA. However, in the samples cured for 3 days, the strengths were rather decreased compared to those cured for 1 day. Furthermore, depending on the type of C_3A, differences in the development of strength at 3 days were confirmed: in the case of the c-C_3A series, enhanced strength was obtained with TIPA application, but an inverse relationship between the amount of TIPA added and the compressive strength was confirmed with the o-C_3A series. These trends could be directly related to the modified hydration behavior of C_3A induced by TIPA.

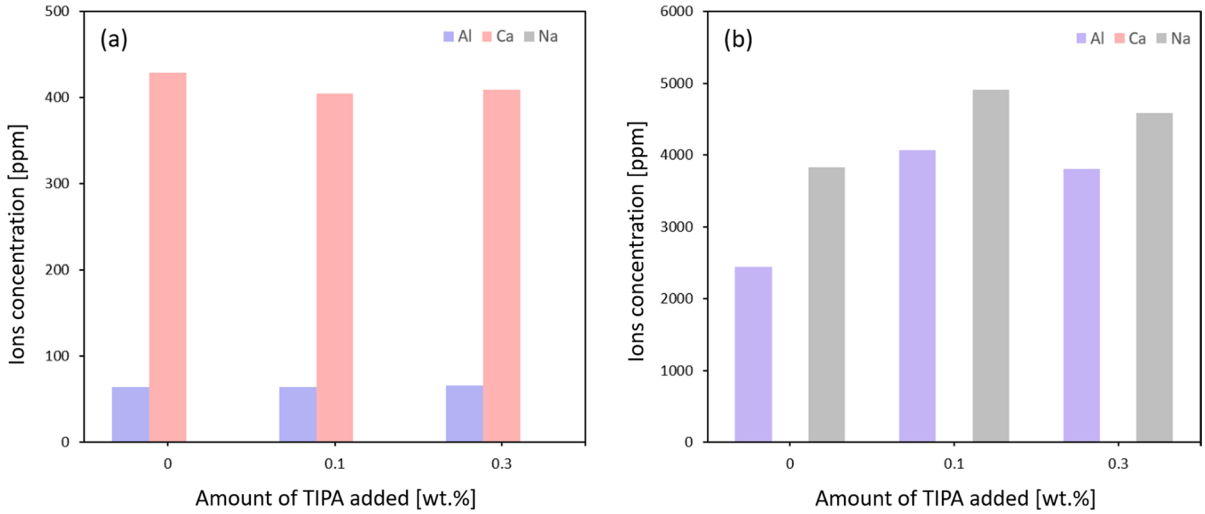

Fig. 4 ICP OES measurements of **a** c-C_3A and **b** o-C_3A series

3.4 ICP OES results

ICP OES results are presented in Fig. 4a, b. This analysis allowed for the evaluation of the reactivity degree of ions. The effect of TIPA on the ion elution degree of C_3A was completely different depending on the type of C_3A. In the case of the c-C_3A series, when the amount of TIPA was increased, the elution amount of Al ions was almost similar, but the detected amount of Ca ions decreased. Meanwhile, with the o-C_3A series, the elution of Al and Na ions remarkably increased with TIPA addition. In particular, it should be noted that the total elution content of ions is also different; the total elution content is lower than 500 ppm with the c-C_3A series, but that of the o-C_3A series is higher than 6,000 ppm. These findings are different from previous studies [4–6], and it could be confirmed that doped-Na is rapidly eluted from o-C_3A.

3.5 Calorimetric results

The impact of TIPA (at doses of 0, 0.1, and 0.3%) on C_3A phases was investigated, and the results are shown in Fig. 5a–d. After water and c-C_3A series were mixed, a substantial amount of heat was released, which improved with increasing amounts of TIPA (Fig. 5a). This result is consistent with the trend found in previous studies, which reported that the reactivity of C_3A in the OPC system is enhanced by TIPA [37, 38]. In contrast, surprising results were observed with the o-C_3A series upon TIPA application (Fig. 5c, d): an accelerated hydration reaction was observed until 10 h, followed by a remarkable heat absorption effect from 1 to 3 days. Consequently, the total released heat decreased compared to the o-C_3A_0% sample. Therefore, to elucidate the aforementioned effects, it is necessary to clarify the variation in the hydration behavior of C_3A that was observed during the measurement time.

3.6 TGA results

TG curves of C_3A paste cured for 1 day and 3 days are presented in Fig. 6a, b. In the present study, weight loss below 180 °C indicated the decomposition of OH-AFm (C_4AH_X) [39], while weight loss between 250 and 280 °C could be attributed to the decomposition of gibbsite (AH_3) [40–43]. Furthermore, the weight loss between 200 and 300 °C indicated the decomposition of C_3AH_6 [44, 45]. Based on the previous studies, the hydration mechanism of the hydrated samples can be estimated.

In the absence of TIPA, a large amount of C_4AH_X phases but a small amount of C_3AH_6 were observed in c-C_3A (Fig. 6a). However, upon the addition of TIPA, a significant amount of C_3AH_6 was confirmed, while C_4AH_X was hardly detected. Furthermore, the amount of C_3AH_6 increased with longer curing

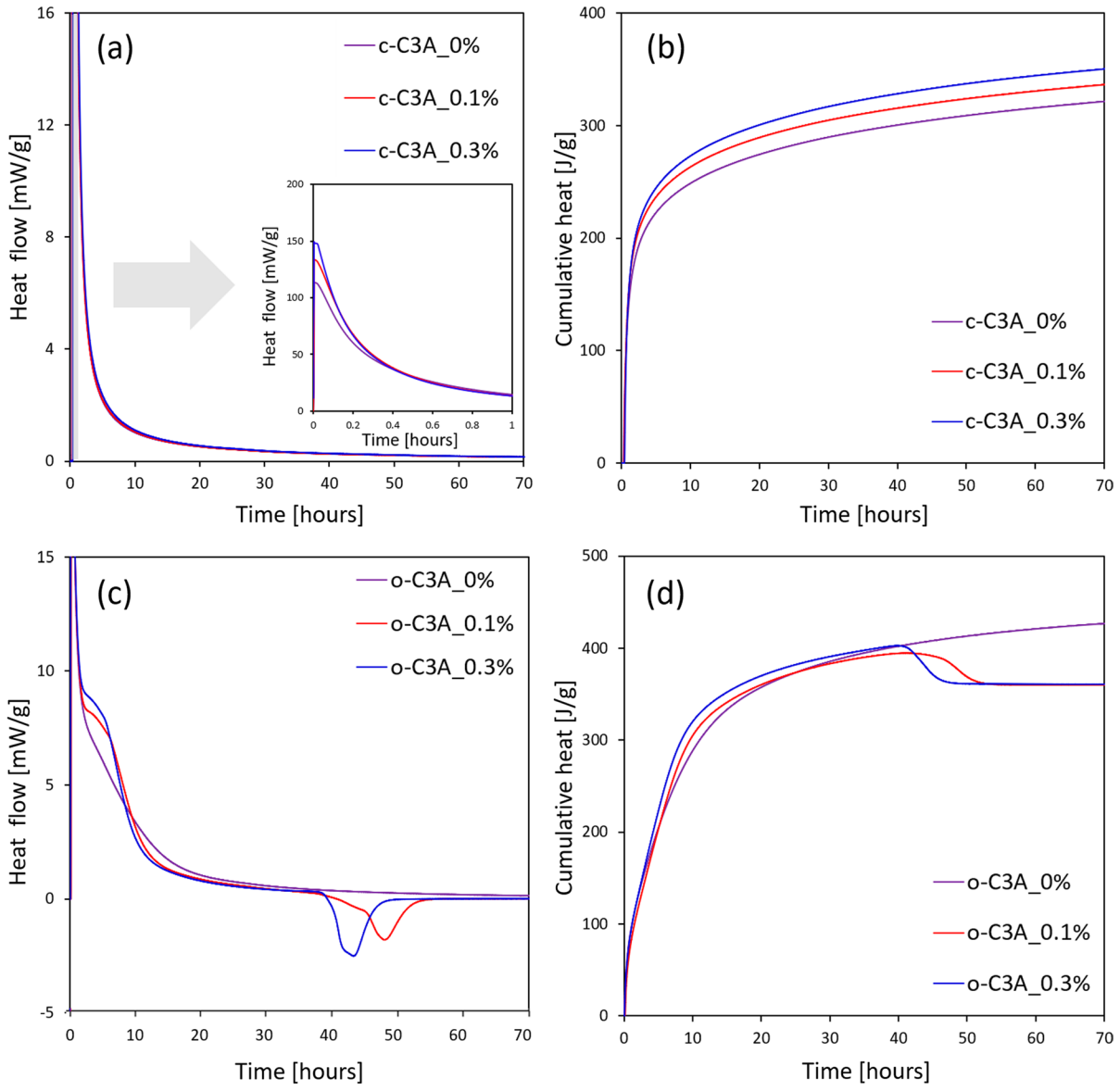

Fig. 5 Hydration heat evolution of the slurry: (**a** and **b**) c-C_3A series and (**c** and **d**) o-C_3A series

durations, from 1 to 3 days. Since C_3AH_6 phase is a fairly thermodynamically stable mineral, the predominantly produced amount of C_3AH_6 phase indicates that C_3A hydration is almost complete [46]. In summary, these results indicate that TIPA acts as an accelerator in the c-C_3A system.

A different trend was observed with the o-C_3A series. In the o-C_3A_0% sample, substantial amounts of both C_3AH_6 and C_4AH_X phases were observed regardless of curing duration. When TIPA was added to o-C_3A, an interesting result was observed: a significant amount of C_4AH_X phases was confirmed in the samples cured for 1 day, but these phases were hardly detected in the samples cured for 3 days (Fig. 6b). Instead, a remarkable amount of C_3AH_6 was obtained, indicating that the phase transitions from C_4AH_X to C_3AH_6 might occur. Although C_3AH_6 phase is stable in an environment of 20 °C, it is commonly reported

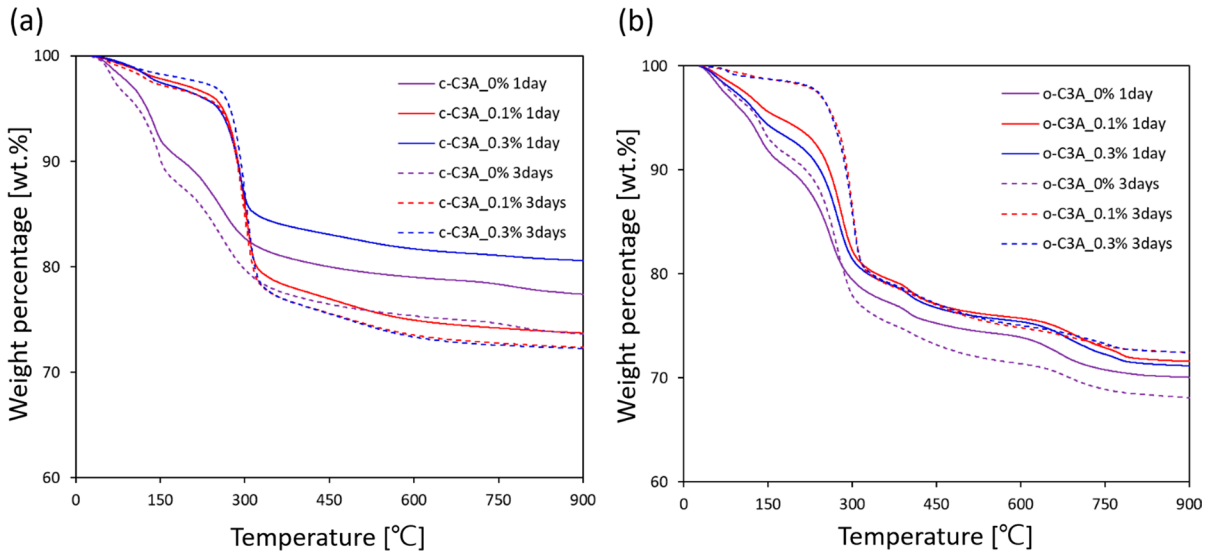

Fig. 6 TG results of **a** c-C_3A and **b** o-C_3A series

that C_4AH_X phases are predominantly produced in short curing durations [6, 47, 48]. Therefore, these findings are not typical trends. Since it is challenging to determine this only with TGA, more detailed explanations will be provided with QXRD results.

3.7 XRD results

The XRD patterns of unhydrated C_3A are presented in Fig. 7a, b). No significant changes in the XRD pattern were observed in the c-C_3A series upon the addition of TIPA, while substantial modifications were observed in the o-C_3A series. Specifically, the peaks located at 33.0° and 33.3° for the o-C_3A series decreased with increasing amounts of TIPA. It is

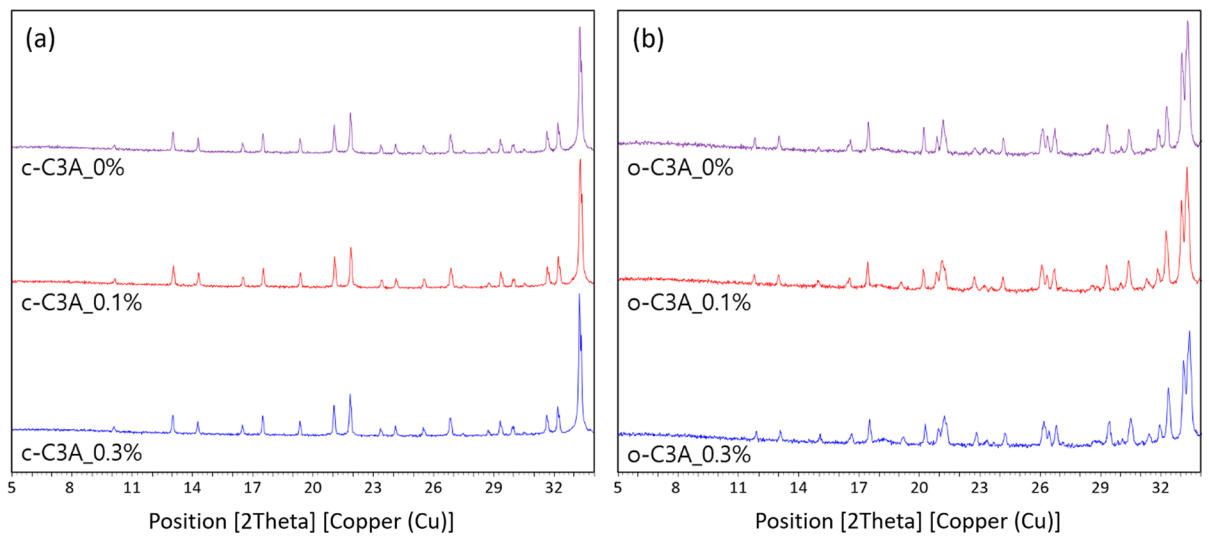

Fig. 7 X-ray diffraction patterns of the investigated C_3A according to the amount of TIPA added: **a** c-C_3A and **b** o-C_3A series

likely that the crystal structure of the minerals was altered due to the combination of grinding program [49]. Further details will be discussed in Sect. 4.2.

The XRD patterns of the hydrated C_3A are presented in Fig. 8a–f. For the c-C_3A_0% sample, a significant amount of C_4AH_X phases was observed. Specifically, the C_4AH_{11} and C_4AH_{13} phases located at 11.8° and 10.5°, respectively, were detected in the sample cured for 1 day (Fig. 8a). After two days, the C_4AH_{13} phase was not observed, but a noticeable amount of C_4AH_{19} phase located at 8.5° was detected. This suggests the rehydration effect of the C_4AH_{13} phase [50]. Meanwhile, upon the addition of TIPA, the hydration mechanism was completely altered, with almost no C_4AH_X phases detected and a significant amount of C_3AH_6 produced instead (Fig. 8c, e).

In the case of o-C_3A_0%, significant amounts of C_4AH_X and C_3AH_6 phases were produced. Similar to the c-C_3A_0% sample, the C_4AH_{11} and C_4AH_{13} phases were also observed in the sample cured for 1 day (Fig. 8b). However, with o-C_3A_0% cured for 3 days, it was clearly detected that not only C_4AH_{19} and C_4AH_{11} phases but also the C_4AH_{13} phase were present. Moreover, interesting results were obtained when TIPA was added. When 0.1% TIPA was added to o-C_3A, the C_4AH_{11} and C_4AH_{19} phases were confirmed in the sample cured for 1 day (Fig. 8d). When the o-C_3A_0.3% sample was cured for 1 day, it was detected that the C_4AH_{13} and C_4AH_{11} phases were present (Fig. 8f). After two days, the C_4AH_{19} and C_4AH_{13} phases were completely decomposed (Fig. 8d, f). It should be noted that there was a difference between the samples cured for 1 day and 3 days; as the curing duration increased from 1 to 3 days, the C_4AH_{19} and C_4AH_{13} phases might be transformed to C_3AH_6 phase, which could be related to the heat absorption effect observed in Sect. 3.5. These findings will be systemically verified with QXRD and thermodynamic database.

4 Discussion

4.1 Effect of TIPA on surface compositions of unhydrated C_3A

In this section, the effects of TIPA on C_3A phases are discussed in relation to carbonation and pre-hydration effects, which are directly related to C_3A reactivity. Variations in the XPS spectra of C 1s were clearly observed and are shown in Fig. 9a, b. As the amount of TIPA added increased, the C 1s spectra decreased, but the Ca 2p spectra showed an anomalous trend Fig. 9c, d. Previous studies have reported that the Ca 2p spectra are less sensitive to changes in composition [34, 36]. As reported in the previous study, the increase in the C 1s peak indicates the formation of monocarboaluminate through the reaction of CO_2 and C_4AH_x in the atmosphere [9]. Moreover, in XPS analysis, given that the measurement encompasses the surface of the C_3A particle (approximately 1 to 10 nm thick) [51], this result suggests that the reaction occurs at the particle surface, and it can be inferred by the addition of TIPA. Therefore, to analyze the carbonation effect quantitatively, it is necessary to compare the relative ratios of the Ca 2p and C 1s spectra.

To investigate the carbonation effect of TIPA on the unhydrated C_3A surface, the relative area ratios of the C 1s and Ca 2p spectra were calculated as presented in Fig. 10a, b) and Table 3 and 4. The C/Ca ratios of C_3A phases without TIPA were calculated to be approximately 0.17 (c-C_3A_0%) and 0.37 (o-C_3A_0%), which is equivalent to being exposed to moist air for approximately 12 h [9]. The calculated values indicate that surface carbonation could be accelerated during the grinding process. On the other hand, it should be noted that the effect was mitigated by the addition of TIPA. This phenomenon can be attributed to the uniform coating of the C_3A surface by TIPA during the grinding process [15]. In particular, this effect was predominantly observed in the c-C_3A series. This is considered to be because the initial reactivity of c-C_3A is relatively lower than that of o-C_3A. Nevertheless, based on the results, it can be concluded that TIPA is effective in inhibiting surface carbonation regardless of the type of C_3A phase.

The binding energies of Al 2p can be used to evaluate the degree of pre-hydration of the C_3A surface. It has been reported that high binding energies in the Al 2p spectra indicate hydrated C-A-H phases [9]. For example, binding energy of 73.8 eV has been reported for C_4AH_{13}, while a range of values between 74.3 and 74.5 eV has been reported for C_3AH_6 [52], which was also observed in the present study. Overall, the addition of TIPA led to decreases in binding energies for both polymorphs (Table 3 and 4, and Fig. 11a, b). Based on these findings, it can be

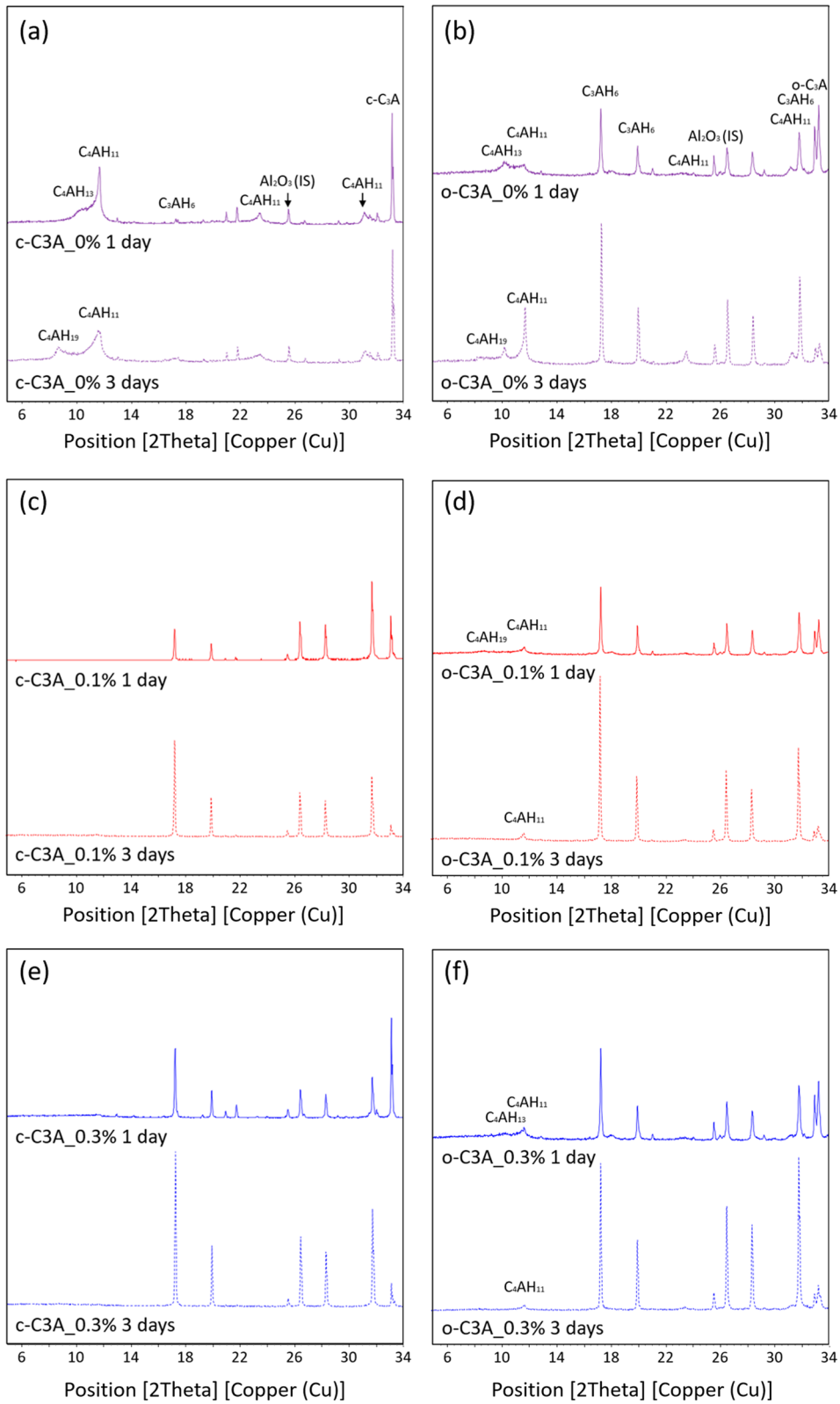
(a)
c-C3A
C4AH11
C4AH13
C3AH6
Al2O3 (IS)
C4AH11
C4AH11
c-C3A_0% 1 day
C4AH11
C4AH19
c-C3A_0% 3 days
(b)
C3AH6
o-C3A
C3AH6
C4AH11
C4AH11
C3AH6
Al2O3 (IS)
C4AH11
o-C3A_0% 1 day
C4AH11
C4AH19
o-C3A_0% 3 days
6 10 14 18 22 26 30 34
Position [2Theta] [Copper (Cu)]
(c)
c-C3A_0.1% 1 day
c-C3A_0.1% 3 days
(d)
C4AH19
C4AH11
o-C3A_0.1% 1 day
C4AH11
o-C3A_0.1% 3 days
(e)
c-C3A_0.3% 1 day
c-C3A_0.3% 3 days
(f)
C4AH11
C4AH13
o-C3A_0.3% 1 day
C4AH11
o-C3A_0.3% 3 days

◂**Fig. 8** XRD patterns of all investigated C_3A (cured for 1 day and 3 days): **a** c-C_3A_0%, **b** o-C_3A_0%, **c** c-C_3A_0.1%, **d** o-C_3A_0.1%, **e** c-C_3A_0.3%, and **f** o-C_3A_0.3%

suggested that although pre-hydration of the C_3A surface was confirmed in all samples, TIPA reduced the degree of pre-hydration to some extent.

4.2 Modifications of crystallographic information of unhydrated C_3A induced by TIPA

Partial modifications of the XRD pattern were observed in the unhydrated c-C_3A and o-C_3A due to the addition of TIPA, as shown in Fig. 12a, b. Specifically, in the c-C_3A series, the peak located at 33.2° slightly increased as the amount of TIPA added increased. However, the opposite trend was observed in the o-C_3A series: the two peaks located at 33.0° and 33.3° decreased as the amount of TIPA added increased. It is well-known fact that variations in crystallographic information are typically observed with grinding programs [53–55]. Therefore, the variations of the XRD patterns induced by the grinding program and TIPA were regarded as partial modifications of the crystal structure.

As presented in Table 5, modifications in the crystal structure of unhydrated C_3A phases were confirmed with TIPA application. Interestingly, completely opposite trends were observed between the c-C_3A and o-C_3A series. With the increase in the amount of TIPA, the lattice parameters of c-C_3A increased, resulting in a massive unit cell volume. Meanwhile, in the case of o-C_3A series, the unit cell parameters decreased with the addition of TIPA, and the unit cell volume also decreased. Previous studies have suggested that these changes may affect the inherent characteristics of the mineral [56, 57]. Therefore, it could be suggested that the hydration properties of C_3A phases changed with the aforementioned effect.

4.3 Variations of hydration behavior of C_3A due to TIPA application

Table 6 and Fig. 13a, b show the quantitative TG and XRD results of all C_3A samples (cured for 1 day and 3 days). The o-C_3A_0% series exhibited a higher degree of hydration compared to the c-C_3A_0% series, and a completely different hydration mechanism was also observed. In the c-C_3A_0% series, significant amounts of C_4AH_X phases were quantified, while in the o-C_3A_0% series, both C_4AH_X and C_3AH_6 were detected. This could be due to the presence of Na^+ ions in o-C_3A, which can affect the hydration behavior by increasing the pH in the paste matrix [9].

Surprisingly, remarkable variations in hydration properties were observed with the addition of TIPA. As mentioned above, significant amounts of amorphous phases (mostly considered to be C_4AH_X phases) were quantified in the c-C_3A_0% sample. However, with the addition of TIPA (i.e., c-C_3A_0.1% and c-C_3A_0.3%), a remarkable amount of C_3AH_6 was quantified. This result is in contrast to what was found in previous studies [58, 59]. In addition, similar modifications of the hydration behavior of o-C_3A were also observed with TIPA application, with C_3AH_6 phase being predominantly produced. However, a clear phase transition from C_4AH_X to C_3AH_6 was observed during the curing period from 1 to 3 days, along with consumption of AH_3 (Fig. 14a, b). From these observations, it can be suggested that C_4AH_X and AH_3 react to produce a significant amount of C_3AH_6. Therefore, it is suggested that the hydration behavior of o-C_3A with TIPA during this particular curing period (1–3 days) can be described by Eq. (3–5). The CEMDATA used for enthalpy calculations is as follows: Gibbsite was used for AH_3, and liquid water was used for H.

Among the thermodynamic analysis results, the positive enthalpy change observed in Eq. (4 and 5) has been verified, indicating an endothermic reaction that absorbs heat from the surroundings [60]. Although only a trivial quantity of C_4AH_{19} was detected in the o-C_3A_0.3% 1 day sample, an enhanced heat absorption effect was observed compared to the o-C_3A_0.1% sample. However, it might be reasonable to observe more endothermic reactions in o-C_3A_0.3% due to its significant content of C_4AH_{13}. Furthermore, this could be attributed to the presence of C_4AH_{19} in a state of poorly crystallinity within the o-C_3A_0.3% 1 day sample [61]. This may be attributed to the partial modifications of the crystallographic information of o-C_3A induced by TIPA, alongside mitigated pre-hydration and/or carbonation effects. These findings hold significance as alkanolamine-based substances are present in nearly all OPC formulations.

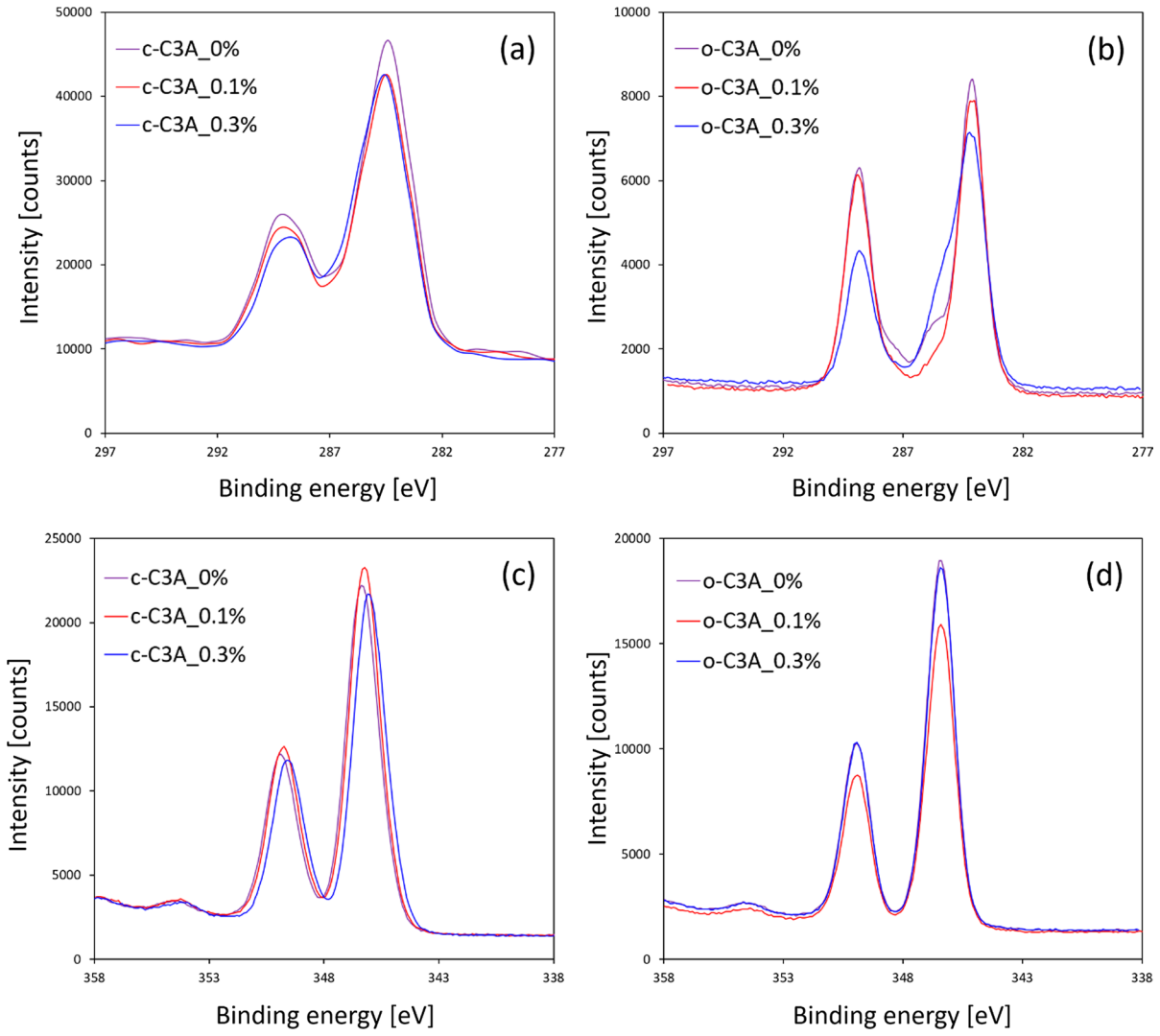

Fig. 9 XPS spectra of C and Ca of unhydrated (**a** and **c**) c-C_3A and (**b** and **d**) o-C_3A series

$$3C_4AH_{11} + AH_3 \rightarrow 4C_3AH_6 + 12H,\ \Delta H_{rxn}: -28,544.07\ J/mol \quad (3)$$

$$3C_4AH_{13} + AH_3 \rightarrow 4C_3AH_6 + 18H,\ \Delta H_{rxn}: +72,789.55\ J/mol \quad (4)$$

$$3C_4AH_{19} + AH_3 \rightarrow 4C_3AH_6 + 36H,\ \Delta H_{rxn}: +191,114.5\ J/mol \quad (5)$$

4.4 Alterations in the structural stability of C_3A composite with TIPA

Figure 15a–d presents the relationship between the total amount of hydration products and compressive strength. It is a well-known fact that compressive strength and the total amount of hydration products are generally proportional. However, for the samples cured for 1 day, the strength improvement was higher in the c-C_3A_0.3% sample, despite the total amount of hydration products being lower compared to the c-C_3A_0% sample (Fig. 15a). This might be due to differences in the produced hydration products and

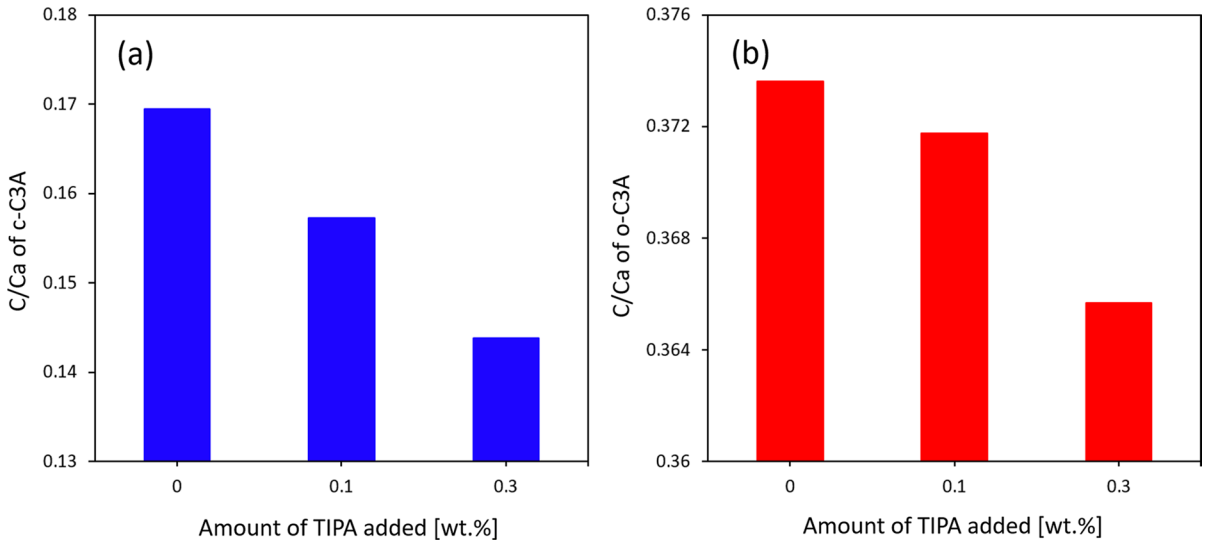

Fig. 10 Normalized ratios of C and Ca of **a** c-C_3A and **b** o-C_3A induced by TIPA

Table 3 Fitting results of XPS spectra of c-C_3A series

Element	Binding energy (eV)		
	c-C_3A_0%	c-C_3A_0.1%	c-C_3A_0.3%
Al 2p	72.93	72.83	72.13
	74.31	74.22	74.00
C 1 s	284.38	284.50	284.32
Ca $2p_{2/3}$	346.63	346.93	346.70

Table 4 Fitting results of XPS spectra of o-C_3A series

Element	Binding energy (eV)		
	o-C_3A_0%	o-C_3A_0.1%	o-C_3A_0.3%
Al 2p	73.34	73.13	73.22
	73.94	73.78	73.85
C 1 s	284.47	284.48	284.51
Ca $2p_{2/3}$	346.57	346.50	346.48
Na 1 s	1,070.69	1,070.62	1,070.57
	1,071.35	1,071.31	1,071.23

their amounts, as well as the ratio among the hydration products (i.e., C_3AH_6, AH_3, C_4AH_X phases) produced by the addition of TIPA. These results suggest that the structural stability of hydrated C-A-H phases might vary.

However, it is difficult to identify a consistent trend between the compressive strength of samples cured for 1 day and 3 days. Although the total amount of hydration products significantly increased in all samples (from 1 to 3 days), the compressive strength decreased instead. In the case of c-C_3A_0% and o-C_3A_0%, the rehydration of C_4AH_X phases was observed, indicating that a phase transition from C_4AH_{13} to C_4AH_{19} occurred [8, 62]. Since the structural stability of C_4AH_X might decrease as the water content increases, this effect could weaken the mechanical properties of the samples cured for 3 days compared to those cured for 1 day. As previously discussed, phase transition effects were observed in all samples with TIPA during the curing duration from 1 to 3 days. When C_4AH_X phases were converted to C_3AH_6 phase, the breaking of initial bonds and transportation of the hydration products occurred [63, 64]. Therefore, the transformation of already formed hydration products during a short period of time could weaken the structural stability of C_3A composites.

5 Conclusions

In this study, two C_3A polymorphs were examined to elucidate the hydration characteristics of "TIPA-C_3A systems". The effects of TIPA on the surface composite and crystal structure of unhydrated C_3A were investigated using XPS and XRD analyses,

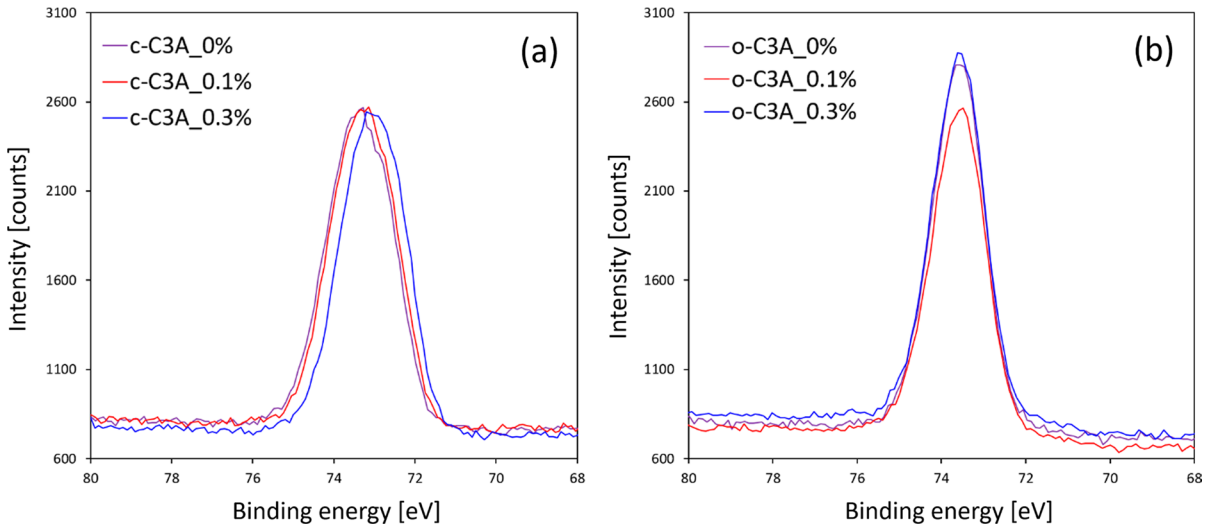

Fig. 11 XPS spectra of Al of **a** c-C_3A and **b** o-C_3A series

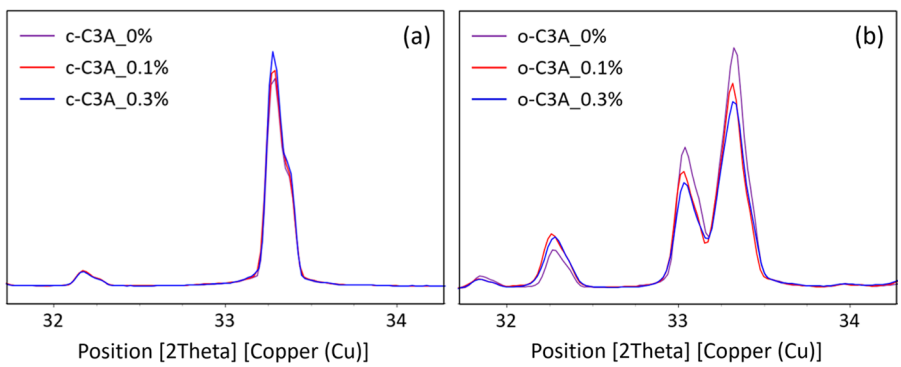

Fig. 12 XRD patterns of the unhydrated **a** c-C_3A and **b** o-C_3A series

Table 5 Profile fitting results of unhydrated c-C_3A and o-C_3A series

	Unit cell parameters			Unit cell volume	Bonding length of Al–O
	a (Å)	b (Å)	c (Å)	Average (Å^3)	Average (Å)
c-C_3A_0%		15.2493		3,546.0549	1.7507
c-C_3A_0.1%		15.2532		3,548.8191	1.7511
c-C_3A_0.3%		15.2534		3,548.9431	1.7511
o-C_3A_0%	10.8626	10.8594	15.1235	1,783.9908	1.7513
o-C_3A_0.1%	10.8527	10.8525	15.1121	1,779.8673	1.7500
o-C_3A_0.3%	10.8521	10.8499	15.1103	1,779.1548	1.7497

respectively. The hydration behavior of C_3A modified due to TIPA was characterized using ICP OES, TGA, and QXRD techniques. In short, the heat absorption behavior in o-C_3A was experimentally confirmed for the first time. Furthermore, its result was thermodynamically supported by the thermodynamic data available in databases like CEMDATA. To optimize various material performance of cement-based materials, tailoring nano-structure of cement mixture is critical which can have much

Table 6 Weight loss and CBW values of C_3A cured for 1 day and 3 days

Sample label	Weight loss at 180 °C (wt%)	Weight loss between 200 and 300 °C (wt%)	CBW (wt%)
c-C_3A_0% 1 day	12.1	8.7	21.0
c-C_3A_0% 3 days	16.0	9.7	24.7
c-C_3A_0.1% 1 day	3.4	15.0	25.1
c-C_3A_0.1% 3 days	4.3	16.0	26.5
c-C_3A_0.3% 1 day	3.7	12.2	18.3
c-C_3A_0.3% 3 days	2.7	14.6	26.7
o-C_3A_0% 1 day	13.1	13.6	26.2
o-C_3A_0% 3 days	11.8	18.1	28.7
o-C_3A_0.1% 1 day	7.0	15.6	24.3
o-C_3A_0.1% 3 days	2.0	15.7	25.2
o-C_3A_0.3% 1 day	8.9	14.8	24.7
o-C_3A_0.3% 3 days	1.9	16.5	25.0

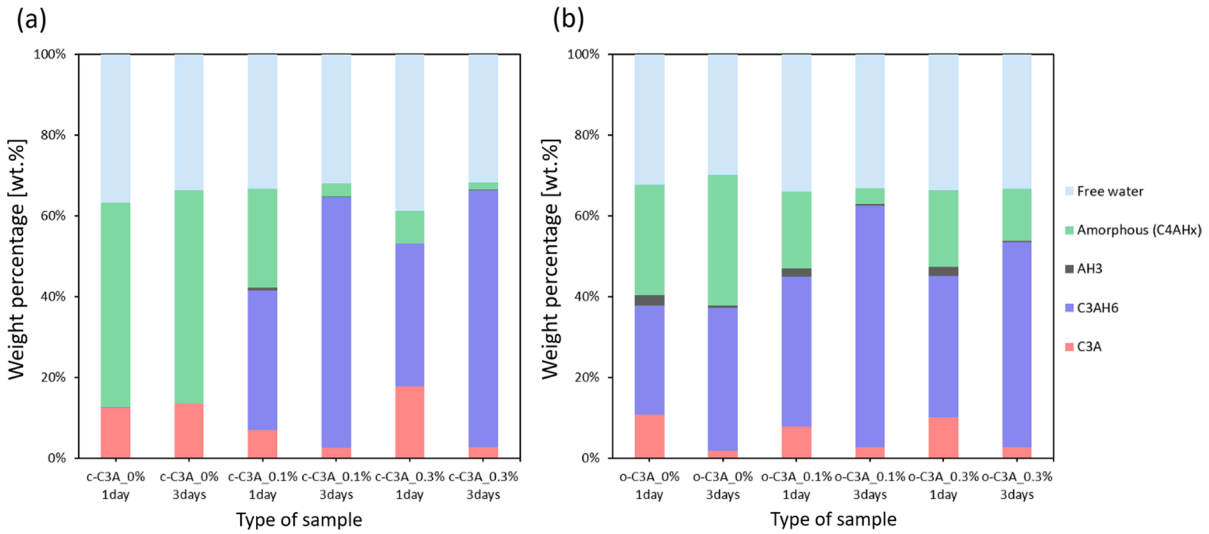

Fig. 13 QXRD results of the **a** c-C_3A and **b** o-C_3A series cured for 1 day and 3 days

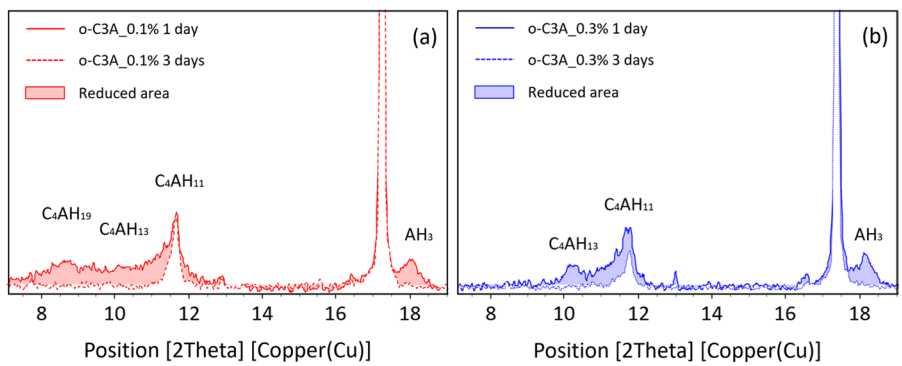

Fig. 14 Phases transition effects of o-C_3A from 1 to 3 days according to TIPA application: **a** o-C_3A_0.1% and **b** o-C_3A_0.3%

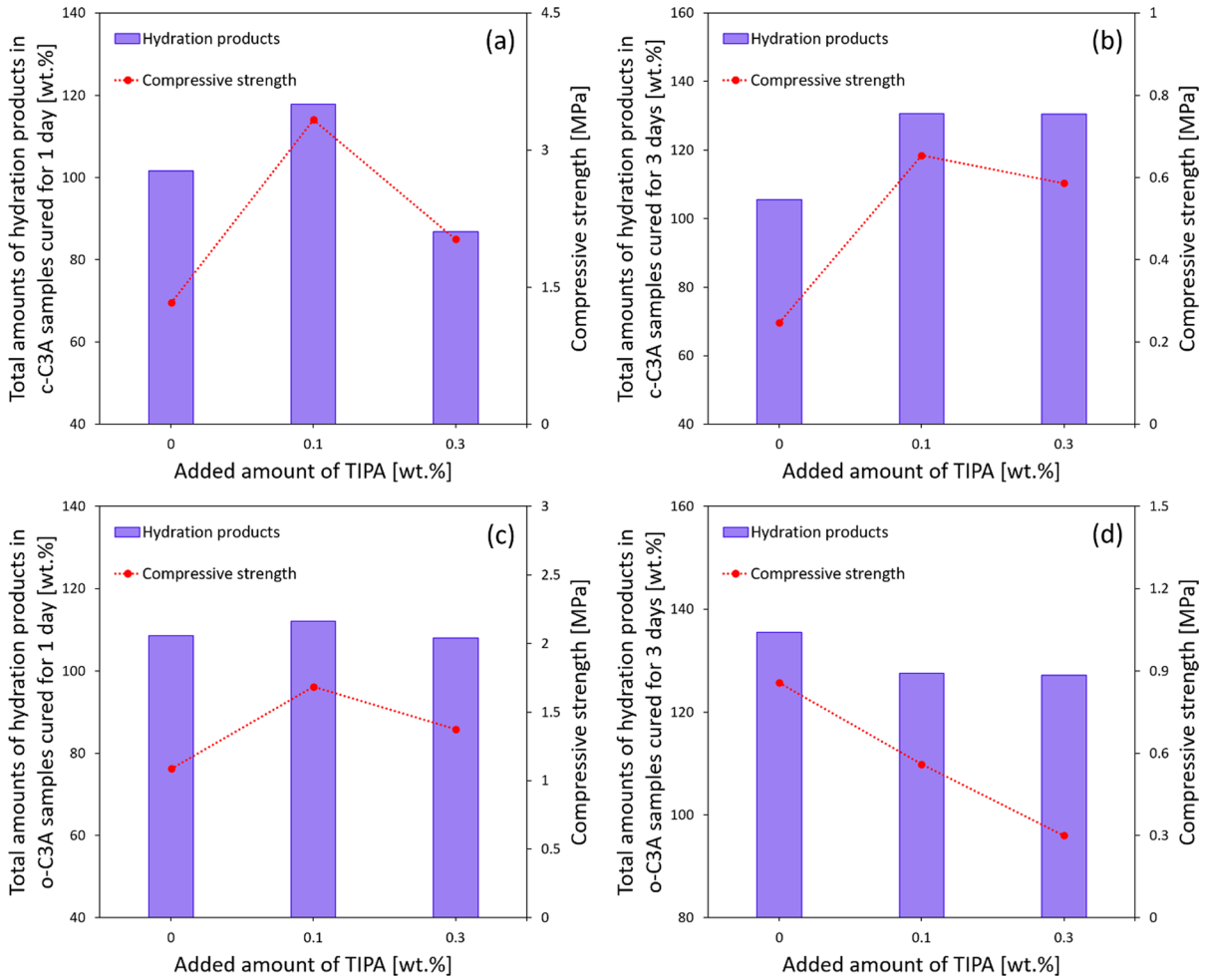

Fig. 15 Relationship between total amounts of hydration products and compressive strength: **a** c-C_3A cured for 1 day, **b** c-C_3A cured for 3 days, **c** o-C_3A cured for 1 day, and **d** o-C_3A cured for 3 days

higher impact on material properties compared to other relatively expensive methods (such as using chemical admixture). In this sense, understanding on the crystallographic changes and resulting hydration characteristics of cement minerals under the use of functional grinding agent is important for the development of suitable grinding agent for cement-based materials.

XPS analysis confirmed pre-hydration and carbonation effects in both C_3A phases during the grinding process. However, these effects were prevented under the use of TIPA. Notably, these effects were more prominent in c-C_3A than in o-C_3A. Since C_3A hydration is closely related to the early hydration properties of OPC, such as setting and hardening, these results can be extended to control the material behavior of OPC. Based on XRD analysis, partial modifications of the crystallographic information of C_3A were observed with the addition of TIPA. This was directly interpreted by changes in the unit cell parameters of C_3A, resulting in variations in the Al–O state.

Aforementioned effects led to significant modification of hydration behavior of C_3A as compared to previously reported research. Despite the short curing period (3 days), the dominant production of C_3AH_6 instead of C_4AH_X phases was confirmed. In particular, the phase transition of C_4AH_X phases to C_3AH_6 was clearly observed in o-C_3A, resulting in an interesting heat absorption

effect which was well explained further by thermodynamic data available in databases like CEMDATA. With these analyses of hydration behavior, the variations in compressive strength were also explained.

Acknowledgements This work was supported by the Industrial Strategic Technical Development Program-Development of manufacturing technology of hardened cement with carbonation curing (RS-2022-00155662, Development of manufacturing and application technology of 1,000 ton/year class hardened cement with carbonation curing) funded by the Ministry of Trade, Industry & Energy (MOTIE, Korea). The Institute of Engineering Research in Seoul National University provided research facilities for this work.

Funding Open Access funding enabled and organized by Seoul National University.

Declarations

Conflict of interest None.

References

1. Boikova AI, Domansky A, Paramonova V, Stavitskaja G, Nikushchenko V (1977) The influence of Na_2O on the structure and properties of 3CaO. Al_2O_3. Cem Concr Res 7(5):483–492
2. Gobbo L, Sant'Agostino Ll, Garcez L (2004) C3A polymorphs related to industrial clinker alkalies content. Cem Concr Res 34(4):657–664
3. Neto JSA, de Matos PR, De la Torre AG, Campos CE, Gleize PJ, Monteiro PJ, Kirchheim AP (2022) The role of sodium and sulfate sources on the rheology and hydration of C3A polymorphs. Cem Concr Res 151:106639
4. Kirchheim AP, Rodríguez ED, Myers RJ, Gobbo LA, Monteiro PJM, Dal Molin DCC, De Souza RB, Cincotto MA (2018) Effect of gypsum on the early hydration of cubic and Na-doped orthorhombic tricalcium aluminate. Materials 11(4):568
5. Stephan D, Wistuba S (2006) Crystal structure refinement and hydration behaviour of doped tricalcium aluminate. Cem Concr Res 36(11):2011–2020
6. Myers RJ, Geng G, Rodriguez ED, da Rosa P, Kirchheim AP, Monteiro PJ (2017) Solution chemistry of cubic and orthorhombic tricalcium aluminate hydration. Cem Concr Res 100:176–185
7. Kirchheim A, Fernàndez-Altable V, Monteiro P, Dal Molin D, Casanova I (2009) Analysis of cubic and orthorhombic C3A hydration in presence of gypsum and lime. J Mater Sci 44:2038–2045
8. Baquerizo LG, Matschei T, Scrivener KL, Saeidpour M, Wadsö L (2015) Hydration states of AFm cement phases. Cem Concr Res 73:143–157
9. Dubina E, Plank J, Black L (2015) Impact of water vapour and carbon dioxide on surface composition of C3A polymorphs studied by X-ray photoelectron spectroscopy. Cem Concr Res 73:36–41
10. Breval E (1977) Gas-phase and liquid-phase hydration of C3A. Cem Concr Res 7(3):297–303
11. Dubina E, Plank J, Black L, Wadsö L (2014) Impact of environmental moisture on C3A polymorphs in the absence and presence of CaSO4· 0· 5 H_2O. Adv Cem Res 26(1):29–40
12. Ramachandran VS (1976) Hydration of cement—role of triethanolamine. Cem Concr Res 6(5):623–631
13. Yilmaz VT, Menek N, Odabasoğlu M (1993) Quantitative determination of triethanolamine in cements. Cem Concr Res 23(3):603–608
14. Heren Z, Ölmez H (1996) The influence of ethanolamines on the hydration and mechanical properties of Portland cement. Cem Concr Res 26(5):701–705
15. Katsioti M, Tsakiridis P, Giannatos P, Tsibouki Z, Marinos J (2009) Characterization of various cement grinding aids and their impact on grindability and cement performance. Constr Build Mater 23(5):1954–1959
16. Gartner E, Myers D (1993) Influence of tertiary alkanolamines on Portland cement hydration. J Am Ceram Soc 76(6):1521–1530
17. Cheung J, Jeknavorian A, Roberts L, Silva D (2011) Impact of admixtures on the hydration kinetics of Portland cement. Cem Concr Res 41(12):1289–1309
18. Sandberg PJ, Doncaster F (2004) On the mechanism of strength enhancement of cement paste and mortar with triisopropanolamine. Cem Concr Res 34(6):973–976
19. Ma S, Li W, Zhang S, Hu Y, Shen X (2015) Study on the hydration and microstructure of Portland cement containing diethanol-isopropanolamine. Cem Concr Res 67:122–130
20. Lu Z, Kong X, Jansen D, Zhang C, Wang J, Pang X, Yin J (2020) Towards a further understanding of cement hydration in the presence of triethanolamine. Cem Concr Res 132:106041
21. Snellings R, Bazzoni A, Scrivener K (2014) The existence of amorphous phase in Portland cements: Physical factors affecting Rietveld quantitative phase analysis. Cem Concr Res 59:139–146
22. Mei K, Cheng X, Gu T, Zheng Y, Gong P, Li B, Zhang C, Zhang L, Dai B (2021) Effects of Fe and Al ions during hydrogen sulphide (H_2S)-induced corrosion of

tetracalcium aluminoferrite (C4AF) and tricalcium aluminate (C3A). J Hazard Mater 403:123928
23. Yamashita T, Hayes P (2008) Analysis of XPS spectra of Fe2+ and Fe3+ ions in oxide materials. Appl Surf Sci 254(8):2441–2449
24. Caruso F, Mantellato S, Palacios M, Flatt RJ (2017) ICP-OES method for the characterization of cement pore solutions and their modification by polycarboxylate-based superplasticizers. Cem Concr Res 91:52–60
25. Maheswaran S, Kalaiselvam S, Karthikeyan SS, Kokila C, Palani G (2016) β-Belite cements (β-dicalcium silicate) obtained from calcined lime sludge and silica fume. Cement Concr Compos 66:57–65
26. Jeong Y, Kang S-H, Kim MO, Moon J (2020) Acceleration of cement hydration from supplementary cementitious materials: Performance comparison between silica fume and hydrophobic silica. Cement Concr Compos 112:103688
27. Kang H, Moon J (2021) Secondary curing effect on the hydration of ultra-high performance concrete. Constr Build Mater 298:123874
28. Jeong Y, Hargis CW, Kang H, Chun S-C, Moon J (2019) The effect of elevated curing temperatures on high ye'elimite calcium sulfoaluminate cement mortars. Materials 12(7):1072
29. Finger L, Cox D, Jephcoat A (1994) A correction for powder diffraction peak asymmetry due to axial divergence. J Appl Crystallogr 27(6):892–900
30. Gualtieri A, Norby P, Hanson J, Hriljac J (1996) Rietveld refinement using synchrotron X-ray powder diffraction data collected in transmission geometry using an imaging-plate detector: application to standard m-ZrO2. J Appl Crystallogr 29(6):707–713
31. Kang H, Lee N, Moon J (2020) Elucidation of the hydration reaction of UHPC using the PONKCS method. Materials 13(20):4661
32. Howard BH (1984) Preliminary data on QXRD analysis of Portland cement and clinker using CeO_2 as the internal standard. Cem Concr Res 14(5):729–740
33. Prziwara P, Kwade A (2021) Grinding aid additives for dry fine grinding processes–Part II: continuous and industrial grinding. Powder Technol 394:207–213
34. Ball MC, Simmons R, Sutherland I (1987) Surface composition of anhydrous tricalcium aluminate and calcium aluminoferrite. J Mater Sci 22:1975–1979
35. Black L, Stumm A, Garbev K, Stemmermann P, Hallam KR, Allen GC (2005) X-ray photoelectron spectroscopy of aluminium-substituted tobermorite. Cem Concr Res 35(1):51–55
36. Barr T (1997) ESCA studies of the coordination state of aluminium in oxide environments. J Chem Soc Faraday Trans 93(1):181–186
37. Huang H, Wang Q, Li X, Zhou H, Yang C-H, Shen X-D (2018) Sulfate adjustment for cement with triisopropanolamine: mechanism of early strength enhancement. Constr Build Mater 182:516–522
38. Li H, Xiang Y, Xu C (2022) Effect of C–S–H seed/PCE nanocomposites and triisopropanolamine on portland cement properties: hydration kinetic and strength. J Build Eng 57:104946
39. Ming X, Li Y, Liu Q, Wang M, Cai Y, Chen B, Li Z (2023) Chloride binding behaviors and early age hydration of tricalcium aluminate in chloride-containing solutions. Cem Concr Compos 137:104928
40. Chang J, Zhang Y, Shang X, Zhao J, Yu X (2017) Effects of amorphous AH3 phase on mechanical properties and hydration process of C4A3S^{-}–CS^{-} H_2–CH–H_2O system. Constr Build Mater 133:314–322
41. MacKenzie K, Temuujin J, Okada K (1999) Thermal decomposition of mechanically activated gibbsite. Thermochim Acta 327(1–2):103–108
42. Vernekar D, Jagadeesan D (2015) Tunable acid–base bifunctional catalytic activity of FeOOH in an orthogonal tandem reaction. Catal Sci Technol 5(8):4029–4038
43. Li M, Li B, Meng F, Liu J, Yuan Z, Wang C, Liu J (2018) Highly sensitive and selective butanol sensors using the intermediate state nanocomposites converted from β-FeOOH to α-Fe_2O_3. Sens Actuators B Chem 273:543–551
44. Mercury JR, De Aza A, Turrillas X, Pena P (2004) The synthesis mechanism of Ca3Al2O6 from soft mechanochemically activated precursors studied by time-resolved neutron diffraction up to 1000 C. J Solid State Chem 177(3):866–874
45. Phrompet C, Sriwong C, Maensiri S, Chindaprasirt P, Ruttanapun C (2018) Optical and dielectric properties of nano-sized tricalcium aluminate hexahydrate (C3AH6) cement. Constr Build Mater 179:57–65
46. Zhang G, Ren Q, He J, Jiang S, Cheng X, Yu Y, Huang S, Zhang C, Zhou M (2021) New understanding of early hydration of C4AF under surface vitrification. Powder Technol 377:372–378
47. Christensen AN, Jensen TR, Scarlett NV, Madsen IC, Hanson JC (2004) Hydrolysis of pure and sodium substituted calcium aluminates and cement clinker components investigated by in situ synchrotron X-ray powder diffraction. J Am Ceram Soc 87(8):1488–1493
48. Black L, Breen C, Yarwood J, Deng C-S, Phipps J, Maitland G (2006) Hydration of tricalcium aluminate (C 3 A) in the presence and absence of gypsum—studied by Raman spectroscopy and X-ray diffraction. J Mater Chem 16(13):1263–1272
49. Dey J, Chatterjee A, Majumdar S, Dippel AC, Gutowski O, Zimmermann Mv, Giri S (2019) Ferroelectric order associated with ordered occupancy at the octahedral site of the inverse spinel structure of multiferroic $NiFe_2$ O_4. Phys Rev B 99(14):144412
50. Fischer R, Kuzel H-J (1982) Reinvestigation of the system C4A. nH_2O C_4A. Co_2. nH_2O. Cem Concr Res 12(4):517–526
51. Matthew J (2004) Surface analysis by Auger and X-ray photoelectron spectroscopy. Briggs D and Grant JT (eds). IMPublications, Chichester, UK and SurfaceSpectra, Manchester, UK, 2003. 900 pp., ISBN 1-901019-04-7, 900 pp, Surface and Interface Analysis 36(13) 1647–1647.
52. Dubina E, Black L, Sieber R, Plank J (2010) Interaction of water vapour with anhydrous cement minerals. Adv Appl Ceram 109(5):260–268
53. Kojdecki MA, Bastida J, Pardo P, Amorós P (2005) Crystalline microstructure of sepiolite influenced by grinding. J Appl Crystallogr 38(6):888–899

54. Kristof E, Juhász A (1993) The effect of intensive grinding on the crystal structure of dolomite. Powder Technol 75(2):145–152
55. Kang H, Lee Y, Lee J, Moon J (2023) Importance of amorphous content, surface energy, and preferred orientation on the accurate quantification of cement minerals in clinkers. J Build Eng 66:105887
56. Redhammer GnJ, Tippelt G, Roth G, Amthauer G (2004) Structural variations in the brownmillerite series $Ca_2(Fe_2-x\ Al\ x)O5$: single-crystal X-ray diffraction at 25° C and high-temperature X-ray powder diffraction (25° C≤ T≤ 1000° C). Am Mineral 89(2–3):405–420
57. Li Z, Yin Y, Rumney JD, Shieh SR, Xu J, Fan D, Liang W, Yan S, Zhai S (2019) High-pressure in-situ X-ray diffraction and Raman spectroscopy of Ca_2AlFeO_5 brownmillerite. High Press Res 39(1):92–105
58. Lothenbach B, Pelletier-Chaignat L, Winnefeld F (2012) Stability in the system $CaO–Al_2O_3–H_2O$. Cem Concr Res 42(12):1621–1634
59. Seligmann P Greening N (1962) New techniques for temperature and humidity control in X-ray diffractometry.
60. Lothenbach B, Kulik DA, Matschei T, Balonis M, Baquerizo L, Dilnesa B, Miron GD, Myers RJ (2019) Cemdata18: a chemical thermodynamic database for hydrated Portland cements and alkali-activated materials. Cem Concr Res 115:472–506
61. Meredith P, Donald A, Meller N, Hall C (2004) Tricalcium aluminate hydration: Microstructural observations by in-situ electron microscopy. J Mater Sci 39:997–1005
62. Baquerizo LG, Matschei T, Scrivener KL, Saeidpour M, Thorell A, Wadsö L (2014) Methods to determine hydration states of minerals and cement hydrates. Cem Concr Res 65:85–95
63. Ramachandran VS, Feldman RF (1973) Significance of low water—solid ratio and temperature on the physicomechanical characteristics of hydrates of tricalcium aluminate. J Appl Chem Biotech 23(8):625–633
64. Collepardi M, Monosi S, Piccioli P (1995) The influence of pozzolanic materials on the mechanical stability of aluminous cement. Cem Concr Res 25(5):961–968